Journal of Inorganic and General Chemistry
ZAAC
Zeitschrift für anorganische und allgemeine Chemie
DOI: 10.1002/zaac.201900347
ARTICLE

Extremely Electron-Poor Bis(diarylmethylium)-Substituted Ferrocenes and the First Peroxoferrocenophane

Larissa A. Casper,[a] Steffen Oßwald,[a] Patrick Anders,[a] Lisa-Catherine Rosenbaum,[a] and Rainer F. Winter*[a]

Dedicated to Professor Manfred Scheer on the Occasion of his 65th Birthday

Abstract. We have prepared and studied extremely electron-poor, deeply colored dicationic 1,1′-bis(diarylmethylium)-substituted ferrocenes $[(\eta^5\text{-}C_5H_4\text{-}CAr_2)_2Fe]^{2+}$ with various aryl substituents as their $[B\{C_6H_3(CF_3)_2\text{-}3,5\}_4]^-$ salts. Due to the strong acceptor substitution, the redox potential for the ferrocene-based oxidation of the anisyl- or 2-methylanisyl-substituted congeners **1b**$^{2+}$ and **1c**$^{2+}$ is close to or even surpasses that of the second oxidation of parent ferrocene, i.e. the $Cp_2Fe^{+/2+}$ couple. The strongly Lewis-acidic character of these complexes is manifest through strong interactions with donor solvents, which lead to a significant reduction of the intensities of the charge-transfer bands in their electronic spectra and to solvatochromism. The reduced forms of the complexes tend to dimerize or oligomerize as revealed by EPR spectroscopy. Direduced **1b** selectively reacts with molecular oxygen to form a peroxo-bis(diarylmethyl)[4]ferrocenophane, which was also characterized by X-ray crystallography.

Introduction

Triarylmethylium (tritylium) substituted ferrocenes constitute the most prominent examples of metal-organic tritylium dyes and were studied early on for their electronic structures. Particular focus was on the ability of the iron nucleus of the ferrocene scaffold to stabilize the positively charged, adjacent methylium center by σ- or π-interactions as expressed by the resonance forms **IV** and **V** in Scheme 1.[1] Such kind of interactions were initially inferred by the 20.7° bending of the CPh_2^+ plane toward the Fe^{2+} ion in the crystallographically determined structure of Fc-CPh_2^+[2] (Fc = ferrocenyl, $(\eta^5\text{-}C_5H_5)Fe(\eta^5\text{-}C_5H_4)$) and by quantum chemical calculations,[3] but later refuted by the notion of a small energy barrier for rotation around the Cp–C^+Ar_2 bond[4] and the generally large dipole moments of ferrocenyl carbenium ions.[1f]

The electron-donating ferrocenyl substituent and the strong dipolar character of such compounds usually lead to intense charge-transfer absorptions in the visible regime of the electronic spectrum (Vis), which are typical of donor-substituted tritylium dyes. Vinylogous or alkynylogous expansion of the ferrocenyl arm of such dyes shifts the corresponding charge-transfer band further red and increases its oscillator strength.[5] In ferrocenyl-tritylium dyes Fc-C^+Ar_2, the CT transitions from the carbocyclic substituents to the methylium center are augmented by an additional, weaker CT band (the HOMO→LUMO transition) concomitant with the direct transfer of electron density from the Fe^{2+} ion to the methylium acceptor. In agreement with this assignment, this band is bleached on oxidation, whereby the ferrocene donor is changed into an electron-poor ferrocenium ion. The same behavior is observed on reduction of the tritylium entity to a trityl radical, which essentially removes its electron-accepting capabilities. Neutral ferrocenyl(diaryl)methyl radicals $FcC^{\bullet}Ar_2$ are prone to dimerize, and an authentic hexaarylethane structure was proposed for these dimers.[6]

Quite surprisingly, no 1,1′-disubstituted, dicationic bis(diarylmethylium)-substituted ferrocenes seem to be known to date. Only the 1,1′-bis(isopropylium)-derivative $[(\eta^5\text{-}C_5H_4CMe_2)_2Fe]^{2+}$ derivative was generated by either protonation and dehydration of the corresponding diol in FSO_3H/SbF_5[7] or protonation of the bis(isopropenyl) derivative with FSO_3H in liquid SO_2 and characterized by NMR spectroscopy,[8] but found to persist only at temperatures below –30 °C. Herein we present the first three representatives of such complexes, bearing aryl substituents of differing electron-donating capabilities. We have probed their electronic properties by means of electrochemistry and UV/Vis/NIR as well as EPR spectroscopic studies on the dications and their reduced and oxidized forms. We also report a unique *ansa*-peroxoferrocenophane, which is formed by the selective reaction of the monoreduced radical cation of the bis(anisyl) derivative with molecular oxygen.

Results and Discussion

Synthesis and Spectroscopic Characterization

The target 1,1′-bis(triarylmethylium)-substituted ferrocenes **1a**$^{2+}$ to **1c**$^{2+}$ were prepared in a two-step procedure analogous to

* Prof. Dr. R. F. Winter
E-Mail: rainer.winter@uni-konstanz.de
[a] Fachbereich Chemie
Universität Konstanz
Universitätsstraße 10
78453 Konstanz, Germany
Supporting information for this article is available on the WWW under **http://dx.doi.org/10.1002/zaac.201900347** or from the author.

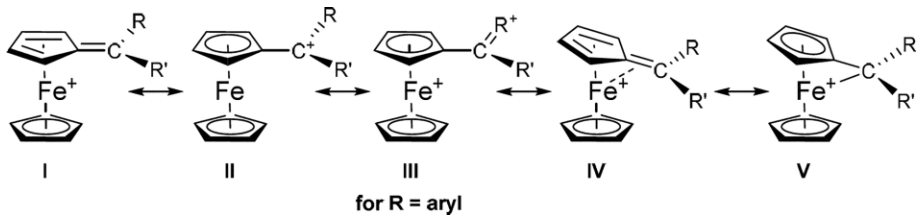

Scheme 1. Resonance formulas of ferrocenyl-substituted methylium cations.

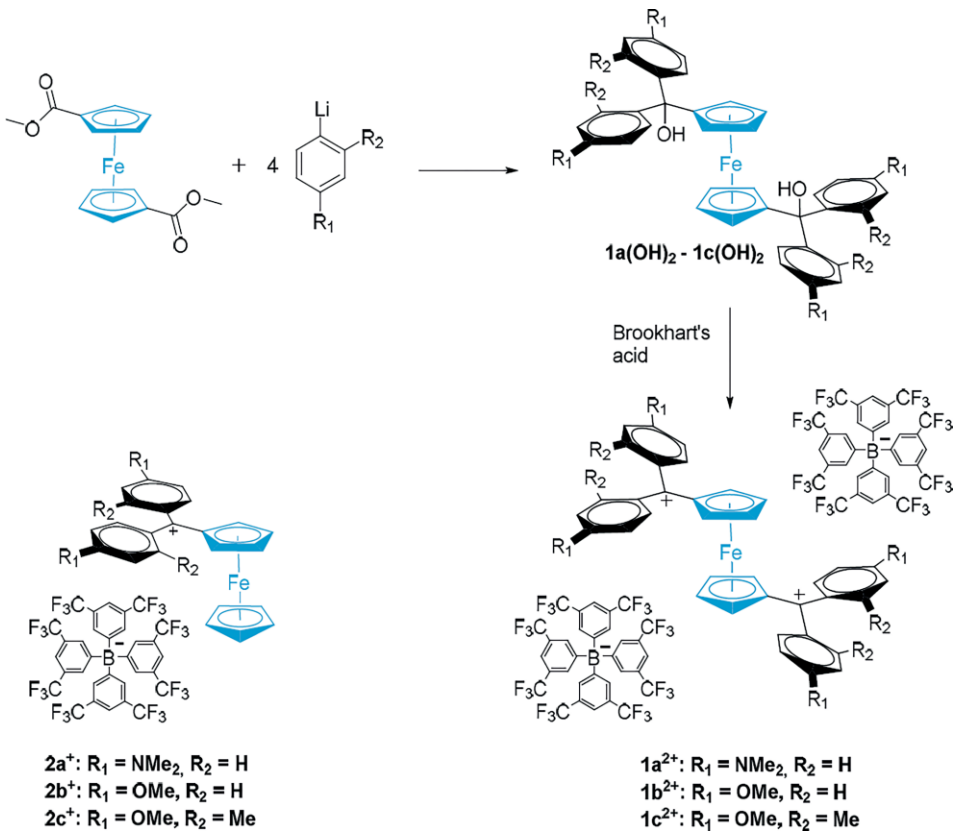

Scheme 2. Synthesis of the 1,1′-bis(triarylmethylium)-substituted ferrocenes $\mathbf{1a^{2+}}$–$\mathbf{1c^{2+}}$ and their monotritylium congeners $\mathbf{2a^{+}}$–$\mathbf{2c^{+}}$.

that employed for the synthesis of their monosubstituted congeners $\mathbf{2a^{+}}$ to $\mathbf{2c^{+}}$ (Scheme 2). Thus, 1,1′-ferrocenedicarboxylic acid dimethyl ester[9] was reacted with ca. 4.2 equiv. of a lithiated arene to provide the corresponding 1,1′-bis(diarylmethylcarbinols) $\mathbf{1a\text{-}(OH)_2}$ to $\mathbf{1c\text{-}(OH)_2}$ after workup. On addition of Brookhart′s acid $H(OEt_2)^+$ $[B\{C_6H_3(CF_3)_2\text{-}3,5\}_4]^-$,[10] an instantaneous color change to blue ($\mathbf{1a^{2+}}$), dark green ($\mathbf{1b^{2+}}$), or dark yellow ($\mathbf{1c^{2+}}$) was observed. The so-dubbed BAr_{F24}^- anion, which was first reported by *Kobayshi* in 1984,[11] is very weakly nucleophilic and has only little ion-pairing capabilities,[6,12] which is both crucial for the stabilization of strong electrophiles such as the present ones. After solvent removal, the corresponding dicationic bis(triarylmethylium)-substituted ferrocenes were obtained as intensely blue, red, or vividly purple solids.

Compound $\mathbf{1a^{2+}}$ provided well-resolved NMR spectra with the characteristic resonance signals of the monosubstituted Cp rings at δ = 5.17 and 4.99 ppm, the two resonances of an AA'BB' spin system for the *para*-substituted arene substituents at δ = 7.57 and 6.69 ppm, and of the *N*-methyl groups at δ = 3.15 ppm in addition to the proton resonances of the $BArF_{24}^-$ anion in their correct integration ratios (see Figure S3, Supporting Information). All these resonances are shifted to lower field when compared to the bis(carbinol) precursor $\mathbf{1a\text{-}(OH)_2}$. Other characteristic assets are the resonance signal of the carbenium centers at δ = 181.1 ppm and the resonances at δ = 127.8 ppm and 84.2 ppm for the adjacent carbon atoms at the aryl and the Cp substituents (see Figures S4, Supporting Information and the Experimental Section). These signals likewise experience substantial low-field shifts with respect to the corresponding carbinol precursor. As expected, the magnitude of this shift is largest for the newly formed carbenium centers, where it amounts to more than 100 ppm. The methylium resonance signal appears nevertheless at a slightly higher field when compared to δ = 188.0 ppm for its monotritylium congener $\mathbf{2a^{+}}$ (Scheme 2).[6] Of the remaining two bis(tritylium)fer-

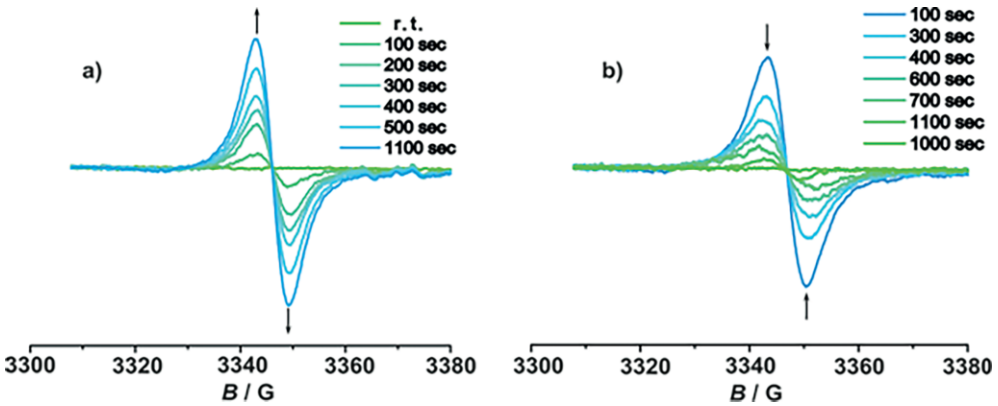

Figure 1. Time-dependent EPR spectra of $\mathbf{1b^{2+}}$ in $CHCl_3$ on (a) warming to 60 °C, and (b) cooling the warm solution to –20 °C.

rocenes, $\mathbf{1b^{2+}}$ provides rather well-resolved resonances in the ^{1}H NMR spectrum at lower concentration levels, which become paramagnetically broadened at higher concentrations (see Figure S6, Supporting Information). This also precluded us from recording meaningful ^{13}C NMR spectra.

In keeping with the presence of small amounts of a paramagnetic component, dicationic $\mathbf{1b^{2+}}$ shows indeed an isotropic, unstructured EPR signal in fluid solution at a *g* value of 2.0086. This signal was initially of only weak intensity at room temperature, but gradually intensified on warming the solution to 60 °C (Figure 1, left) and remained at a rather constant intensity level on cooling back to room temperature. Further cooling to temperatures of –20 °C or below, however, induces a gradual decrease of the signal intensity until the initial level is reached (Figure 1, right). The entire process can be cycled several times. Such reversible intensity changes combined with a hysteretic behavior point to the existence of a thermally accessible paramagnetic state along with a substantial activation barrier connecting this state to the diamagnetic ground state.

A likely explanation for this unusual behavior is thermal equilibration between the native 1,1'-bis(diarylmethylium)ferrocene form $(\eta^5\text{-}Ar_2C^+\text{-}C_5H_4)Fe^{II}(\eta^5\text{-}C_5H_4\text{-}C^+Ar_2)$ and its $(\eta^5\text{-}Ar_2C^+\text{-}C_5H_4)Fe^{III+}(\eta^5\text{-}C_5H_4\text{-}C^{\bullet}Ar_2)$ valence tautomer, where the positive charge has shifted from a triarylmethylium site to the ferrocene nucleus (Scheme 3, top). This renders one of the former triarylmethylium centers a trityl-type radical. As ferrocenium ions are EPR inactive under these conditions, only the trityl component of this biradical is detected by EPR spectroscopy. This valence tautomer was computationally modeled as the triplet state of $\mathbf{1b^{2+}}$. Our quantum chemical calculations produced indeed substantial spin densities on the ferrocene nucleus and the methyl(ium) carbon atoms (Figure 2, left). Complex $\mathbf{1b^{2+}}$ thus complements Veciana′s ferrocenyl-perchlorotriphenylmethyl radicals, which were found to equilibrate with their zwitterionic ferrocenium-perchlorotriphenylmethanide isomers.[13] These two kinds of systems are compared in Scheme 3. They mainly differ in the identity and charge state of the triarylmethyl(ium)-based acceptor units, i.e. cationic Ar_2C^+ in $\mathbf{1b^{2+}}$ vs. neutral $-C_6Cl_4-{}^{\bullet}C(C_6Cl_5)_2$ in Veciana′s systems.

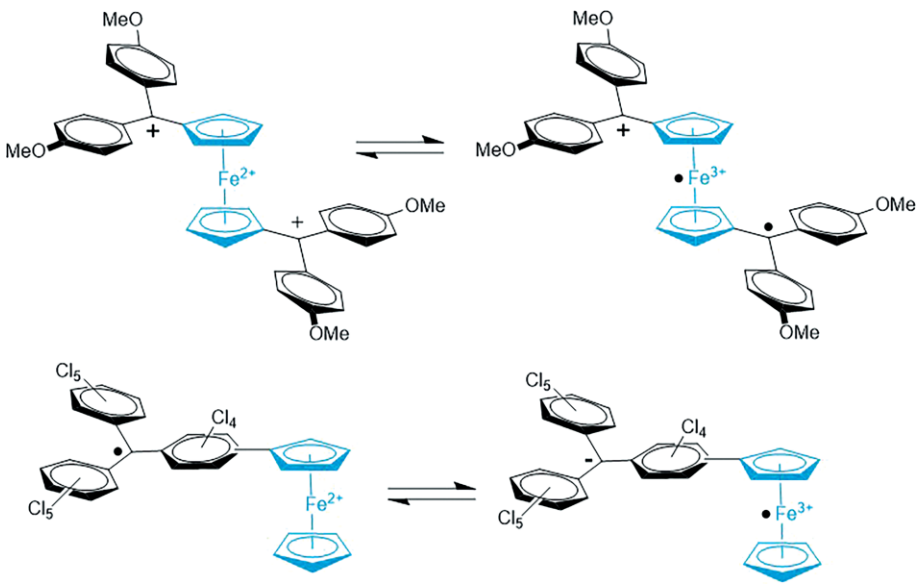

Scheme 3. Valence tautomeric forms of complex $\mathbf{1b^{2+}}$ (top) and of perchlorotriphenyl-substituted ferrocene (bottom).

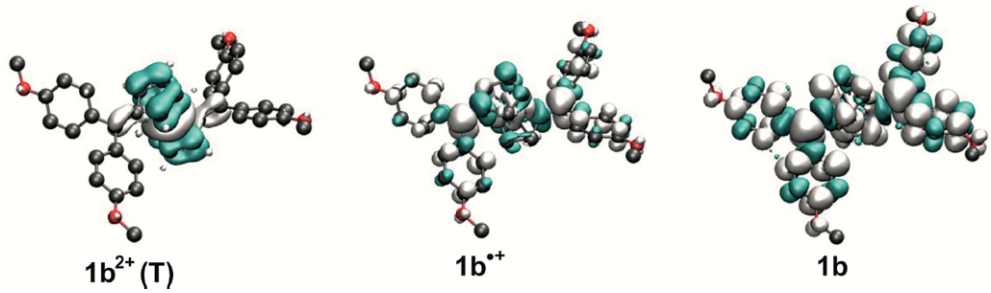

Figure 2. DFT-calculated spin densities for $\mathbf{1b}^{2+}$ in its triplet state (left), monoreduced $\mathbf{1b}^{\bullet+}$ (middle) and neutral **1b** (right).

Neither meaningful NMR nor EPR spectra were, however, obtained for complex $\mathbf{1c}^{2+}$, such that its formation was only verified by UV/Vis spectroscopy. As expected from their vivid colors, all three complexes present intense electronic transitions in their Vis spectra. Their electronic absorption spectra are compared in Figure 3. Like in the solid state, solutions of the complexes in CH_2Cl_2 are intensely blue ($\mathbf{1a}^{2+}$) or purplish red ($\mathbf{1b,c}^{2+}$). The electronic spectrum of $\mathbf{1a}^{2+}$ is dominated by a strong band (ε = 85000 $M^{-1}{\cdot}cm^{-1}$) at 653 nm, which, in analogy to its monotritylium analog $\mathbf{2a}^{+}$ (Scheme 2) is caused by charge-transfer (CT) from the electron-rich 4-dimethylaminophenyl substituents to the carbenium acceptor (the so-called x-band). As a token of the increased acceptor strength owing to the presence of two tritylium-type acceptors, this band is red-shifted by 1130 cm^{-1} (i.e. from 608 nm) when compared to the monotritylium-substituted counterpart $\mathbf{2a}^{+}$. The expected CT transition originating from the substituted Cp ring as the donor (y-band) is presumably associated with the weaker feature at 530 nm, which is present in the spectra of all three complexes. No Fe→tritylium CT band (the so-called y_M-band) is, however, observed; it is likely hidden underneath the intense main band of $\mathbf{1a}^{2+}$.

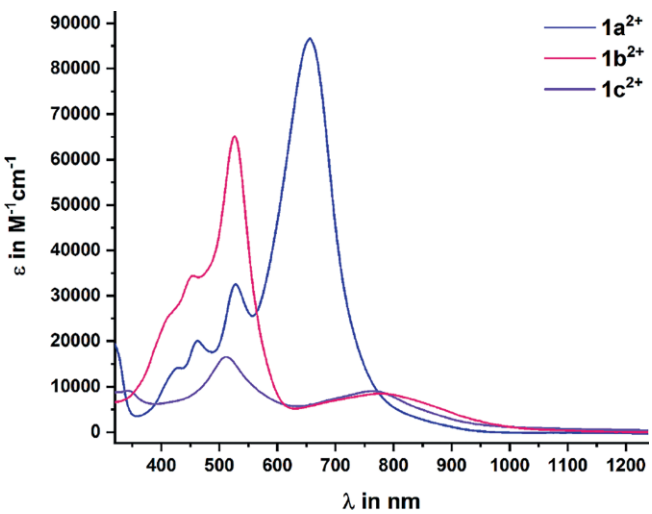

Figure 3. UV/Vis spectra of the bis(triarylmethylium)-substituted ferrocenes in CH_2Cl_2.

In contrast, Vis spectra of complexes $\mathbf{1b,c}^{2+}$ with anisyl or 2-methyl-4-methoxyphenyl substituents at the tritylium center, show a y_M band at 799 nm (ε = 9500 $M^{-1}{\cdot}cm^{-1}$) or at 765 nm (ε = 9900 $M^{-1}{\cdot}cm^{-1}$, Figure 3). According to our TD-DFT calculations, this absorption is associated with charge-transfer from mainly the Fe $d_{x^2-y^2}$ orbital to the empty *p*-orbitals at the methylium carbon atoms. A second feature with a similar character, but differing in the identity of the Fe d donor orbital (d_{z^2}), is observed as a shoulder on the high-energy side of the first y_M band at ca. 630 nm for $\mathbf{1b}^{2+}$ or at ca. 690 nm for $\mathbf{1c}^{2+}$. The main absorption feature of $\mathbf{1b}^{2+}$ is an intense (ε = 65000 $M^{-1}{\cdot}cm^{-1}$), structured peak with a main maximum at 525 nm and separate shoulders at 485 nm and 457 nm. According to our TD-DFT calculations and in agreement with the behavior of other triarylmethylium dyes, these bands are assigned as the combined x- and y-bands with concomitant CT from the donor-substituted aryl rings or the attached Cp ligand to the methylium centers.[14] Figure 4 shows the calculated spectrum and the charge-density differences associated with the individual excitations of complex $\mathbf{1b}^{2+}$. The Vis spectrum of $\mathbf{1c}^{2+}$ differs from that of $\mathbf{1b}^{2+}$ mainly in that the intensity of particularly the x,y bands at 513 nm is greatly diminished. This is a likely result of a larger torsion of the sterically more hindered 2-methyl-4-methoxyphenyl rings with respect to the plane of the methylium acceptors.

Complexes $\mathbf{1b}^{2+}$ and $\mathbf{1c}^{2+}$ show a remarkable solvatochromic behavior. While giving purplish red solutions in CH_2Cl_2 and nitromethane, their solutions in *N*- or *O*-donor solvents like acetone, methanol, THF, Et_2O, CH_3CN, or pyridine assume a grass-green to orange-yellow color. The observable color impressions and absorption spectra of equally concentrated solutions in various solvents are collected in Figure 5; for details to the band positions and absorptivities see Table S1 (Supporting Information). Of note are the greatly diminished absorptivities of all CT bands in any donor solvent. This indicates strong interactions between Lewis-basic solvent molecules and the Lewis-acidic methylium centers of the solute, which reduce the electron-accepting capabilities of the latter. The decrease of the band intensities consequently follows, at least on a qualitative level, the Gutmann donor number *DN*. The latter is defined as the negative value of ΔH^0 in $kcal{\cdot}mol^{-1}$ for adduct formation between an electron pair donor with $SbCl_5$ in a highly diluted solution of 1,2-dichloroethane.[15] The stronger quenching of the bands in $\mathbf{1c}^{2+}$ when compared to $\mathbf{1b}^{2+}$ is consistent with an increased Lewis-acidity of the methylium centers in the former complex as a result of a lower

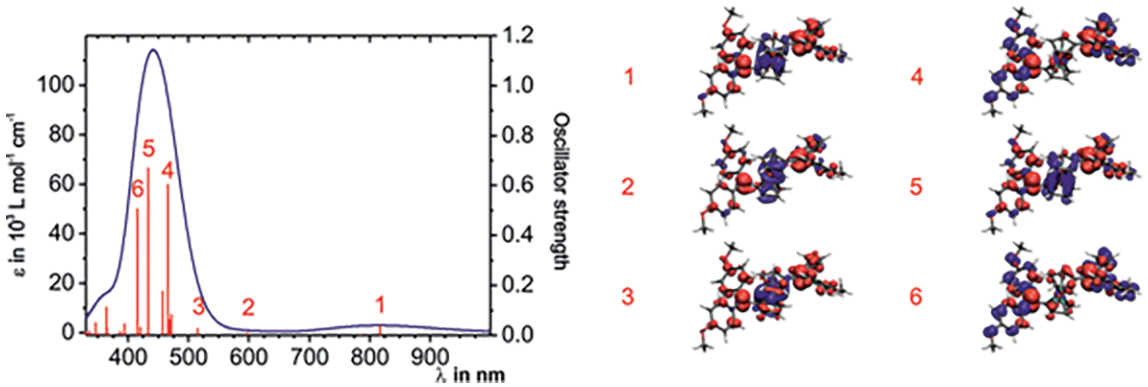

Figure 4. Left: TD-DFT calculated absorption spectrum of complex $\mathbf{1b}^{2+}$; right: electron density difference plots (blue: decreasing electron density, red: increasing electron density) for the most important transitions.

stabilization by the more twisted aryl substituents. Complex $\mathbf{1a}^{2+}$, where the positive charges at the methylium carbons are rather well stabilized by the strongly electron-donating $Me_2NC_6H_4$ substituents, shows a strongly attenuated solvatochromism, changing its color from deep blue in CH_2Cl_2 or nitromethane to dark green in THF or MeOH.

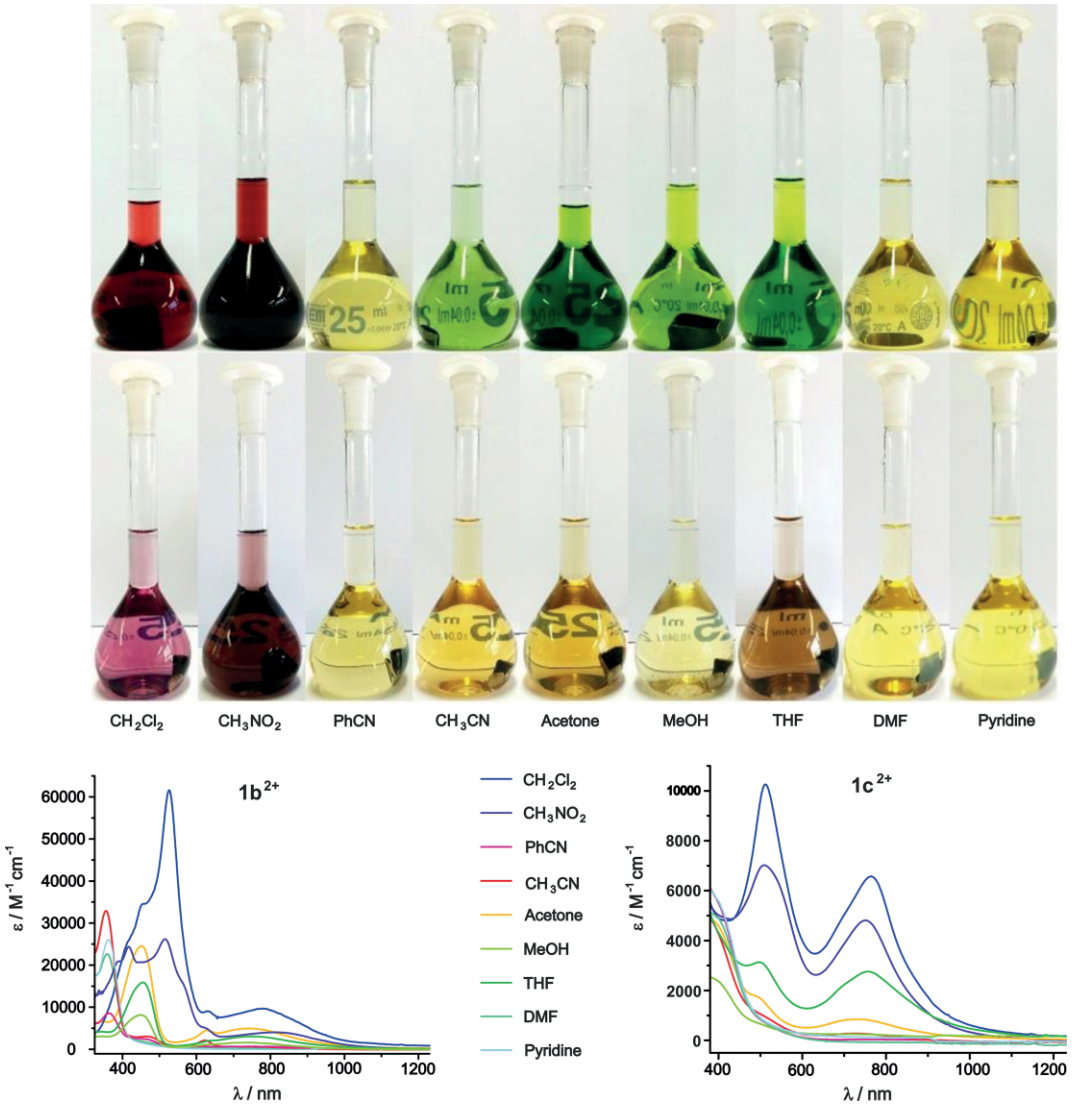

Figure 5. Solvatochromism of complexes $\mathbf{1b}^{2+}$ (top and bottom left) and $\mathbf{1c}^{2+}$ (middle and bottom right).

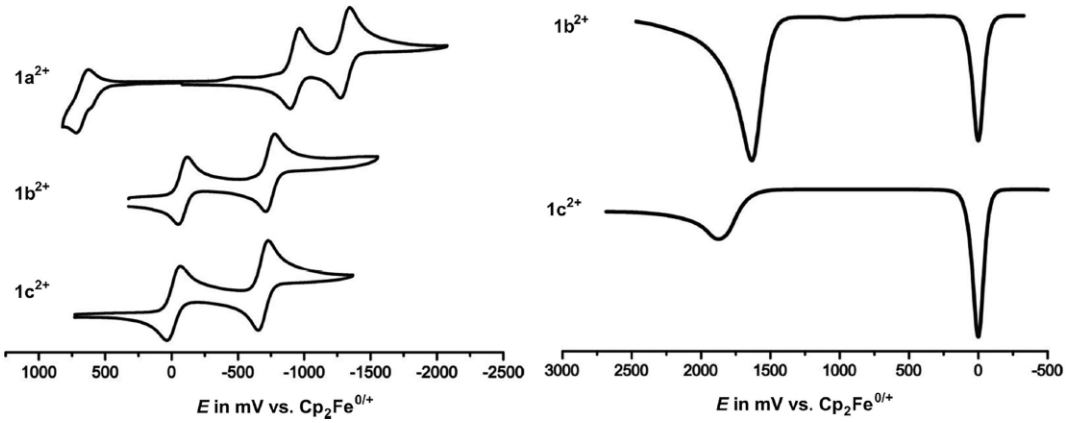

Figure 6. Left: Cyclic voltammograms of complexes $\mathbf{1a^{2+}}$ to $\mathbf{1c^{2+}}$ in CH_2Cl_2/NBu_4BAR_{F24} (0.02 M) at room temperature at a scan rate v = 100 mV·s^{-1}. Right: Square wave voltammograms of complexes $\mathbf{1b^{2+}}$ and $\mathbf{1c^{2+}}$ in $SO_{2(l)}$ at –20 °C with 0.02 M NBu_4BAR_{F24}. The peak at 0 mV is due to the internal $Cp_2Fe^{0/+}$ redox standard.

Electrochemical Studies

The redox properties of the bis(diarylmethylium)-substituted ferrocenes were probed by cyclic and square wave voltammetry. The results of this study are shown in Figure 6; pertinent data are compiled in Table 1. All complexes show two consecutive one-electron reductions for the stepwise transformations of the cationic triarylmethylium to neutral triarylmethyl substituents, i.e. the $CpAr_2C^{+/\bullet}$ couples (Figure 6, left). The splitting of half-wave potentials $\Delta E_{1/2}$ amounts to 405 mV for $\mathbf{1a^{2+}}$ and increases to 670 mV in $\mathbf{1c^{2+}}$ and to 740 mV in $\mathbf{1b^{2+}}$. In every instance, the first reduction wave appears anodic of the first reduction of the corresponding monosubstituted diarylmethylium ferrocenes $\mathbf{2a^{+}}$ to $\mathbf{2c^{+}}$ (Table 1), which is a clear token of the decreased electron density of the tritylium acceptors. The magnitude of the shift between the first reduction of complexes $\mathbf{1a^{2+}}$ to $\mathbf{1c^{2+}}$ and those of their corresponding counterparts $\mathbf{2a^{+}}$ to $\mathbf{2c^{+}}$ increases with decreasing electron-donating capabilities of the aryl substituents. It thus becomes larger the more the effect of changing an electron-donating neutral ferrocenyl entity in complexes **2a**–**2c** to an electron-accepting, cationic (η^5-C_5H_4)Fe(η^5-C_4H_4-CAr_2^+) substituent in complexes **1a**–**1c** is felt by the methylium acceptors and is not compensated by the other aryl substituents. One should note here that, in $\mathbf{1a^{2+}}$ and $\mathbf{2a^{+}}$, the 4-$Me_2NC_6H_4$ substituents are stronger donors than ferrocenyl, while ferrocenyl is the strongest donor in complexes $\mathbf{2b^{+}}$ and $\mathbf{2c^{+}}$. Again, a larger torsion of the 2-methyl-4-methoxyphenyl substituents of $\mathbf{1c^{2+}}$ as compared to the anisyl residues of $\mathbf{1b^{2+}}$ is held responsible for the finding that $\mathbf{1c^{2+}}$ is considerably easier to reduce than $\mathbf{1b^{2+}}$ despite the nominally stronger donor properties of the aryl substituents in $\mathbf{1c^{2+}}$. This effect is even amplified with respect to the corresponding monosubstituted analogs $\mathbf{2b^{+}}$ and $\mathbf{2c^{+}}$ (Table 1).

In the CH_2Cl_2/NBu_4BAr_{F24} electrolyte, the expected oxidation of the central ferrocene constituent can only be observed for the least electron-poor congener $\mathbf{1a^{2+}}$ as a reversible wave at $E_{1/2}$ = 670 mV against the $Cp_2Fe^{0/+}$ couple. This process, however, lies outside the accessible potential range of this electrolyte for the other two complexes. It could nevertheless be observed as a broad square-wave peak at 1640 mV ($\mathbf{1b^{2+}}$) or 1870 mV ($\mathbf{1c^{2+}}$) in liquid SO_2, using NBu_4BAr_{F24} as the supporting electrolyte (Figure 6, right). With such positive redox potentials, $\mathbf{1b^{2+}}$ and $\mathbf{1c^{2+}}$ seem to be the electron-poorest ferrocenes reported to date, including other multiacceptor-substituted ferrocenes such as 1,1′-dicyanoferrocene ($E_{1/2}$ = 865 mV), 1,1′,2,2′,4,4′- and 1,1′,2,2′,3,3′-hexakis(pentafluorophenylferrocene) ($E_{1/2}$ = 940 mV and 951 mV, respectively), 1,1′,3,3′-tetra(methoxycarbonyl)ferrocene ($E_{1/2}$ = 900 mV)[16] and even 1,1′,2,2′-tetraformylferrocene ($E_{1/2}^{0/+}$ = 1145 mV).[17] In fact, their $E_{1/2}$ values nearly match or even

Table 1. Electrochemical data [a) b)] for all complexes.

Complex	Reductions				Oxidation	
	$E_{1/2}$ (0/+)	ΔE_p (0/+)	$E_{1/2}$ (+/2+)	ΔE_p (+/2+)	$E_{1/2}$ (2+/3+)	ΔE_p (2+/3+)
$\mathbf{1a^{2+}}$	–1340	57	–935	57	670	89
$\mathbf{1b^{2+}}$	–880	70	–140	70	1640 [c)]	–
$\mathbf{1c^{2+}}$	–690	70	–20	100	1870 [c)]	–
	(0/+)	(0/+)			(+/2+)	(+/2+)
$\mathbf{2a^{+}}$	–1160	57			490	91
$\mathbf{2b^{+}}$	–780	57			830	180
$\mathbf{2c^{+}}$	–740	72			870	224

a) Potentials in mV (± 3 mV) in CH_2Cl_2 at T = 293(± 3) K relative to the $Cp_2Fe^{0/+}$ couple ($E_{1/2}$ = 0.000 V). Supporting electrolyte NBu_4^+ [B{$C_6H_3(CF_3)_2$}]$_4^-$. b) Data for complexes $\mathbf{2a^{+}}$ to $\mathbf{2c^{+}}$ from reference[6]. c) Potentials were determined by square wave voltammetry in liquid SO_2 at T = 253(± 3) K relative to the $Cp_2Fe^{0/+}$ couple ($E_{1/2}$ = 0.000 V) with NBu_4^+ [B{$C_6H_3(CF_3)_2$}]$_4^-$ as the supporting electrolyte.

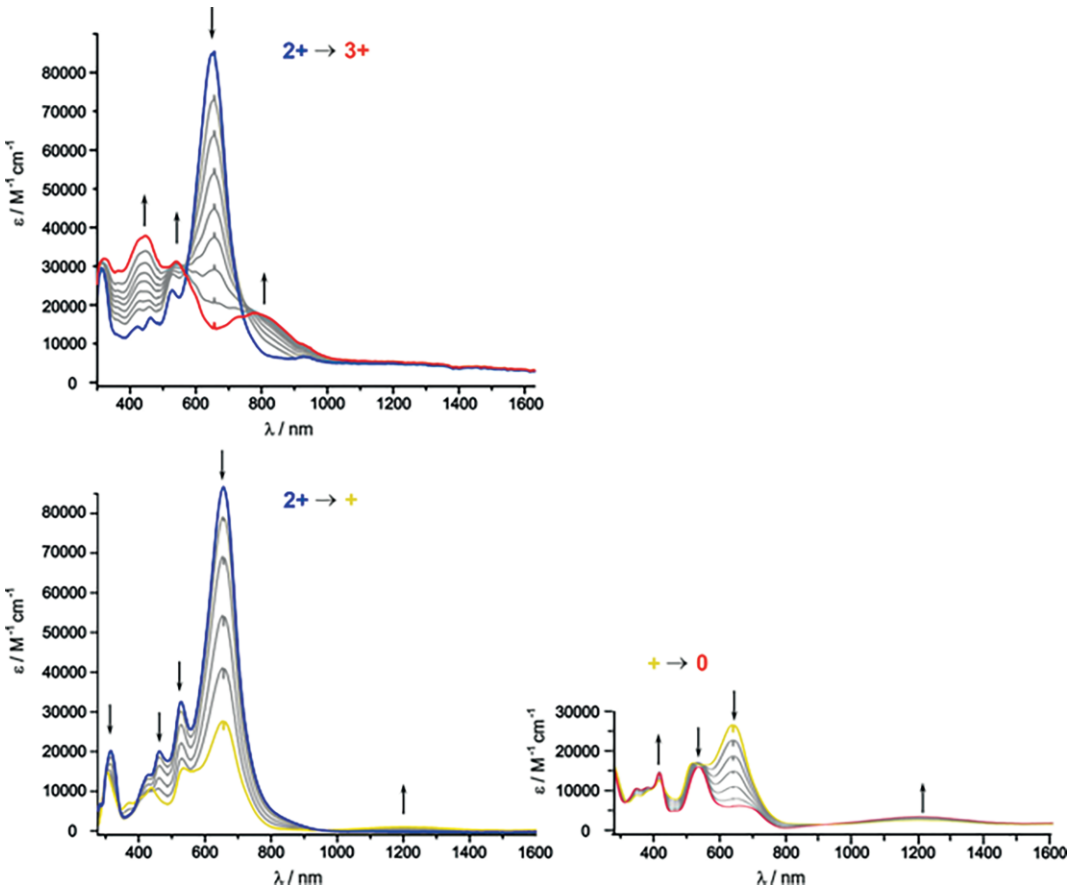

Figure 7. Spectroscopic changes during oxidation (top) as well as the first (bottom left) and second (bottom right) reductions of complex $\mathbf{1a}^{2+}$ (1,2-$C_2H_4Cl_2$ / NBu_4BAr_{F24} (0.02 M) at room temperature).

surpass that of 1710 mV for the *second* oxidation of parent ferrocene (i.e. the $Cp_2Fe^{+/2+}$ couple) under similar conditions.[18]

Spectroscopic Investigations on Some Oxidized and Reduced Forms

The three reversible redox processes of $\mathbf{1a}^{2+}$ provided us with the opportunity to probe for the spectral changes in the Vis/NIR spectra concomitant with these transformations. The results of this study are depicted in Figure 7. On one-electron oxidation, the prominent Vis band of $\mathbf{1a}^{2+}$ at 653 nm is bleached and gives way to less intense bands peaking at 790 nm, 543 nm, and 450 nm. The lower-energy bands are very likely associated with CT from the $C_6H_4NMe_2$ donors to the methylium and ferrocenium acceptor entities. The red-shift of the 790 nm band with respect to that in $\mathbf{1a}^{2+}$ is in line with an inner array of three interconnected strong electron acceptors after ferrocene oxidation.

The two consecutive one-electron reductions likewise bleach the prominent x-band of $\mathbf{1a}^{2+}$ to ultimately leave two bands at 540 nm and 439 nm. By inference from their mono-triarylmethylium-substituted congeners, for which a similar behavior was observed, these bands are assigned as a mixed transition within the ferrocene nucleus and a 1,1′-ferrocenediyl→$CAr_2^{\bullet}$ CT transition (λ = 540 nm) and as π→π* transitions within the trityl chromophore (λ = 439 nm).[6] Of note is the absence of an electronic transition at low energy specific for any radical cation with one neutral $Ar_2C^{\bullet}$ and one cationic Ar_2C^{+} substituent attached to the same ferrocene-1,1′-diyl scaffold (see also Figures S9 and S10, Supporting Information for the results of such studies on complexes $\mathbf{1b,c}^{2+}$). In view of the substantial half-wave potential splitting for the individual reductions one would expect such a charge transfer absorption between differently charged pendants, may it occur through space or via the ferrocene coupling unit. Figure S11 (Supporting Information) displays a possible structure, which would allow for CT through space. Electronic transitions of this kind are well-known for π-stacked mixed-valent donor/acceptor dyads comprising of the reduced and the oxidized forms of a planar, π-conjugated electrophore (so-called pimers).[19] Only during the reduction of $\mathbf{1a}^{2+}$ a suspicious feature was observed as a weak band ($\varepsilon \approx 1000\ M^{-1}{\cdot}cm^{-1}$). This band was, however, found to persist during the second reduction and is hence not specific to $\mathbf{1a}^{\bullet+}$.

The reduced forms of complexes $\mathbf{1a}^{2+}$ and $\mathbf{1b}^{2+}$ were also investigated by EPR spectroscopy. Singly reduced radical cations $\mathbf{1a}^{\bullet+}$ and $\mathbf{1b}^{\bullet+}$ were generated by reacting the dicationic precursors with slightly less than 1 equiv. of cobaltocene in order to avoid overreduction. EPR spectra of these samples

were measured in CH_2Cl_2 solutions in the temperature range of 20 °C to –40 °C or of 20 °C to –60 °C, respectively. As shown in Figure 8, both paramagnetic species display an isotropic signal without any resolved hyperfine splitting at *g* values of 2.0115 (**1a**$^{\bullet+}$) or 2.0301 (**1b**$^{\bullet+}$). Both values are slightly larger than that of ca. 2.003 expected for ordinary trityl radicals,[20] but similar to those of e.g. the triferrocenylmethyl, phenyldiferrocenylmethyl, the ferrocenyl-ruthenocenylmethyl, or the ferrocenyl-diruthenocenylmethyl radicals.[21] DFT-calculated spin densities (Figure 2, middle) show indeed large contributions of the ferrocene-1,1'-diyl entity to the singly occupied molecular orbital (SOMO) of **1b**$^{\bullet+}$.

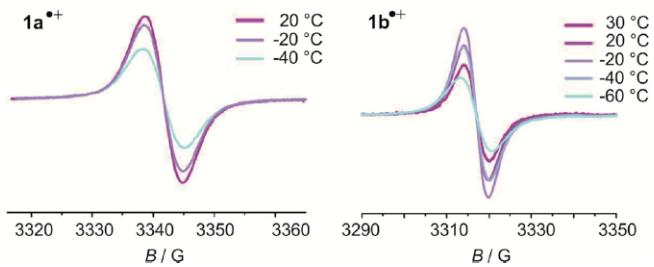

Figure 8. EPR spectra of monoreduced radical cations **1a**$^{\bullet+}$ (left) and **1b**$^{\bullet+}$ (right).

During these studies we also noted an odd temperature-dependence for both radical cations. Thus the intensity of the EPR signal of **1a**$^{\bullet+}$ steadily and reversibly decreases upon cooling. This is just the opposite of the normal Curie behavior as expressed by Equation (1), where *g* denotes the isotropic *g* value of the compound, μ_B is Bohr′s magneton, B_0 the magnetic field strength and k_B is the Boltzmann′s constant. According to this equation, the population of the thermally excited state (decreasing value of ΔN) is expected to diminish with decreasing *T*, and this, in turn, should lead to larger signal intensities for samples with equal spin concentrations as *T* is lowered. Such odd behavior was already observed for reduced samples of triarylmethylium-substituted ferrocenes **2a**$^+$ to **2c**$^+$ and traced to the formation of hexaarylethane-type dimers.[6] The same obviously applies here. We however note that the reduction in signal intensity upon cooling is less pronounced for cationic **1a**$^{\bullet+}$ as compared to **2a**$^{\bullet}$, which is reasonably expected as a consequence of electrostatic repulsion between the positively charged CAr_2^+ pendants of such a dimer. This holds to an even larger degree for radical cation **1b**$^{\bullet+}$, whose signal intensity initially increases on lowering *T*, complying with the normal Curie-behavior, but then decreases upon cooling to even lower temperatures. We thus conclude that dimerization only commences to a noticeable degree at temperatures of or below –20 °C. This can be seen as a token of a lesser delocalization of the positive charge at the remaining tritylium site onto the aryl substituents, which is in full agreement with our electrochemistry data.

$$\Delta N \approx N \frac{g\,\mu_B}{2\,k_B}\frac{B_0}{T} \qquad (1)$$

Fully reduced **1a**, generated by treating **1a**$^{2+}$ with an excess over 2 equiv. of cobaltocene, proved unfortunately too reactive to be reliably characterized by EPR spectroscopy. In the case of **1b**, however, an indicative EPR signal was obtained and its *T* dependence was likewise studied. The results are shown in Figure 9. Diradical **1b** produces two different isotropic signals at *g* values of 2.0283 and of 2.0144. The former value falls close to that of 2.0301 observed for **1b**$^{\bullet+}$. On progressive cooling to lower *T*, this signal gradually decreases in intensity, while that of the signal at higher field first increases and then stays rather constant. We tentatively assign the signal at *g* = 2.0283 to the dissociated diradical and the one at *g* = 2.0144 to a diradical dimer or higher oligomers. We also note that, in contrast to cationic **1b**$^{\bullet+}$, but in agreement with neutral **2b**$^{\bullet}$, dimerization already sets in at or slightly below room temperature as shown by the slight intensity decrease of the low-field EPR resonance in the *T* interval of 20 °C to 0 °C.

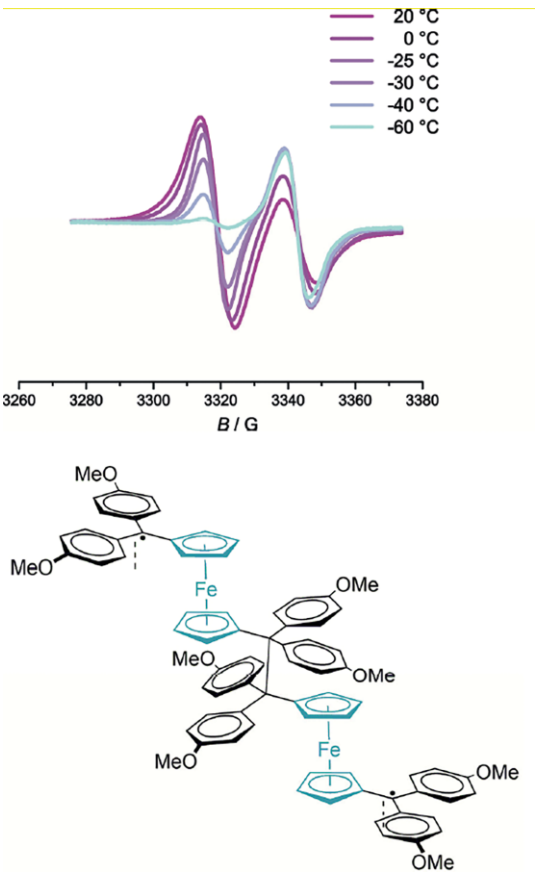

Figure 9. *T*-dependent EPR spectra of reduced **1b** and proposed oligomer formation by spin pairing.

Reactivity Studies of 1b: Formation and Characterization of a Unique Peroxo-[4]ferrocenophane

During attempts to reduce **1b**$^{2+}$ to its radical cation on a preparative scale with Cp^*_2Fe ($E_{1/2}$ = –550 mV) as a selective reductant and without protection from the atmosphere, we observed a fading of the solution color from deep red to greenish yellow. Extraction of the solid obtained after solvent evaporation with *n*-hexane provided a dark yellow solution and a green, insoluble residue, which was not characterized further.

The ^{1}H NMR spectrum of the product obtained from the soluble fraction after solvent removal consists of four separate AB doublets at δ = 7.86, 7.35, 6.90, and 6.52 ppm for the *para*-disubstituted anisyl rings, integrating as 4 protons each, 4 broad singlet resonances at δ = 5.11, 4.21, 4.03, and 3.91 ppm for the Cp protons with an integral of 2 H each, and two singlets, each accounting for 6 H, for the methoxy protons at δ = 3.33 and 3.22 ppm, along with minor impurities (Figure S12, Supporting Information). This pattern of resonance signals indicates the formation of a new 1,1′-disubstituted ferrocene derivative with C_2 symmetry. A pure product was obtained, when 2 equiv. of cobaltocene were added to a CH_2Cl_2 solution of **1b**$^{2+}$ inside a glovebox and stirred for some min before the reaction vessel was taken out of the glove box and left stirring open to the air overnight. Workup as before gave the pure compound in quantitative yield after evaporation of the solvent. The ESI mass spectrum of this product showed the molecular ion peak at *m*/*z* = 699.1925, which matches with an adduct of **1b** with one molecule of oxygen and one proton (Figure S14, Supporting Information). Crystallization of this compound by slow evaporation of a saturated solution in CH_2Cl_2 afforded yellow blocky crystals that proved suitable for X-ray structure determination. As shown in Figure 10, the newly formed product is a neutral peroxo-[4]ferrocenophane **1b-O$_2$** (only one of the two enantiomers of the racemic pair in the crystal is shown; for details of the data collection and refinement, the cell parameters and the bond lengths and bond angles see Tables S2 to S4, Supporting Information).

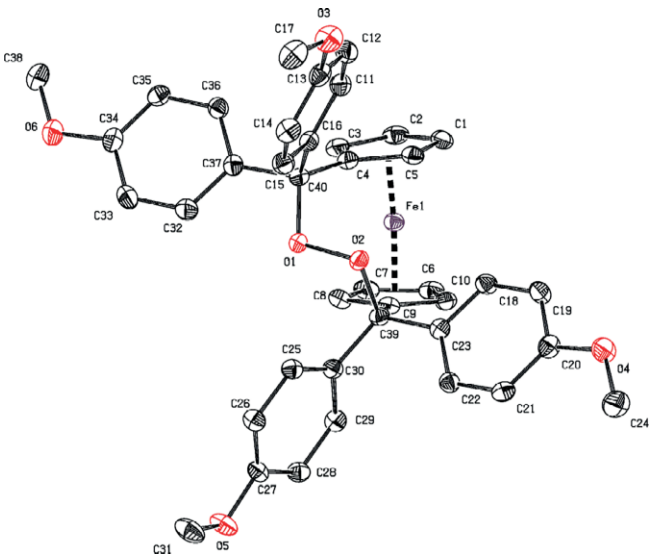

Figure 10. Molecule structure of one enantiomer of **1b-O$_2$** as determined by X-ray crystallography. Hydrogen atoms are removed for reasons of clarity. Ellipsoids are displayed at a 50 % probability level.

In **1b-O$_2$** the former trityl carbon centers and the O atoms of a molecule of O_2 have combined to form a –C–O–O–C– bridge, which interconnects the two Ar_2C– pendants of the upper and lower Cp decks. Within the four-atom linkage bond lengths of 1.526(2) and 1.529(2) Å for the C_{Cp}–C, 1.454(2) and 1.464(2) Å for the C–O, and 1.4789(16) Å for the O–O bonds, bond angles C–O–O of 108.1(1) and 107.0(1)°, and a dihedral angle of –134.2° at the peroxo group are observed. The two Cp decks assume a staggered conformation with a rotation angle of 39.3° (average values C_{Cp}–$Cp_{centroid}$–$Cp_{centroid}$–C_{Cp}) and are tilted by a 7.2°, which indicates that the four-atom C–O–O–C hinge induces an only moderate strain. The C atoms at the hinges are at a closer distance of 3.271 Å as compared to 3.438 Å or 3.540 Å at the opposite, open side of the [4]ferrocenophane structure. This is mirrored by differences in Fe–C_{Cp} bond lengths, which range from 2.0229(18) to 2.0356(19) Å for the C atoms at or in the immediate vicinity of the hinge to 2.067(2) and 2.0667(19) Å at the open side.

We note a close structural similarity to the corresponding 1,1′-bis(diphenyl)peroxo-[4]rhodocenophanium cation, which has a tilt angle of 5.5° between the cyclopentadienyl ligands, C_{Cp}–C–, C–O–, and O–O bond lengths of 1.531(6)/1.521(6) Å, 1.454(4)/1.458(4) Å, and 1.487(4) Å as well as a dihedral angle C–O–O–C of 144.9°.[22] The latter compound and three more derivatives with other, 4-substituted aryl substituents were obtained from the reaction of homoleptic Rh^I complexes [(η^4-C_5H_4=C(C_6H_4R-4)$_2$Rh]$^+$ (R = H, Cl, OMe, Me) bearing 6,6-diphenylfulvene ligands with air.[22–23] Besides the doubly linked (η^5-C_5H_4CPh{(C_2H_4)(O-O)}CPh(η^5-C_5H_4)Fe,[24] the aforementioned [4]rhodocenophanium cations seem to be the only peroxo-[4]metallocenophanes in the literature. It should be noted, though, that aerial oxidation of the trityl radical to the corresponding peroxide was noted as early as in 1903 in one of the first treatises on this compound.[25]

The tilt of 7.2° in **1b-O$_2$** is larger than that of 0.7° to 2.8° found in [4]ferrocenophanes with butane-1,4-diyl or 2-oxo-butane-1,4-diyl bridges. All-carbon-bridged [4]ferrocenophanes even show the larger interplanar C···C distance at the hinge.[26] Such conformational differences result from the much smaller angle between the Fe–O–O and the Cp planes of 11.4° and 15.1° of **1b-O$_2$** as compared to values of 49.0° to 70.6° for interplanar angles Fe–C–C/Cp in the all-carbon bridged counterparts, i.e. from more "upright" conformations of the inner –C_2H_4– or –C(O=)–CH_2– connectors as opposed to a rather flat-lying peroxo group. Similar or even larger tilts of up to 16.0° were observed in [4]ferrocenophanes with fluorinated all-carbon bridges,[27] or in a [4]ferrocenophane with a –CH_2N(Ph)–C($COOMe)_2CH_2$– connector (6.5°).[28]

In further explorations of direduced **1b** we also investigated its reactivity with acetylene-1,4-dicarboxylic acid dimethylester, styrene, CS_2, NO, water and methanol under a protective atmosphere of dinitrogen. From the product mixtures formed in these reactions, known 6,6-dianisylfulvene[23,29] and the unsymmetrically substituted (η^5-$C_5H_4C(C_6H_4OMe)_2OH$)Fe(η^5-$C_5H_4C(C_6H_4OMe)_2H$) (**1b-HOH**, for NMR and ESI mass spectra see Figures S15 to S17, Supporting Information) as the product of water addition were identified besides various, but smaller amounts of **1b-O$_2$**. The latter is obviously formed by the trapping of **1b** with adventitious oxygen. Notably, no polymer formation was observed during the reaction of **1b** with styrene. The release of a 6,6-disubstituted fulvene from a 1,1′-(η^5-$C_5H_4C^{\bullet}R_2)_2$Fe diradical is just the opposite reaction to that observed by *Tacke* and co-workers in their studies on bis(ful-

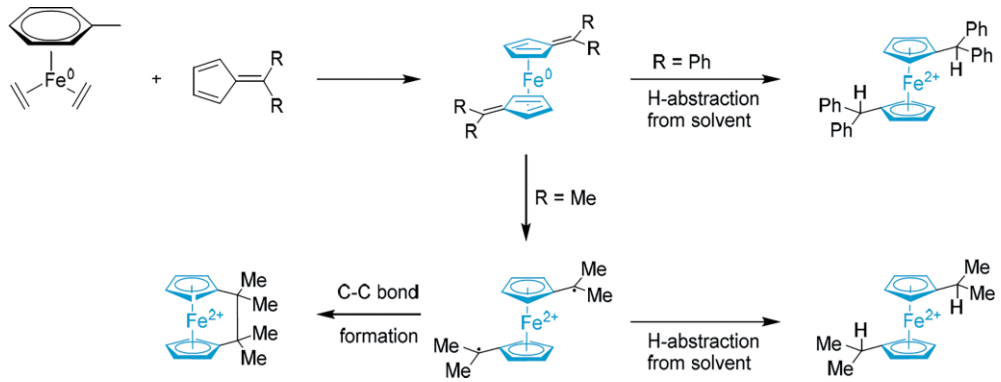

Scheme 4. Formation and reactions of bisfulvene iron(0) complexes.[30]

vene) iron(0) derivatives of 6,6-dimethyl- and 6,6-diphenylferrocene. The latter can either undergo hydrogen atom abstraction from the solvent or, in the case of methyl substituents, C–C bond formation to a [2]ferrocenophane (Scheme 4).[30]

Summary and Conclusions

We report on three 1,1'-bis(diarylmethylium)-substituted ferrocenes of the type $[\{\eta^5\text{-}C_5H_4C(C_6H_4R\text{-}4)\}_2Fe]^{2+}$ [R = NMe_2 (**1a**$^{2+}$); R = OMe (**1b**$^{2+}$)] and $[\{\eta^5\text{-}C_5H_4C(C_6H_3(CH_3\text{-}2)(OMe\text{-}4))\}_2Fe]^{2+}$ (**1c**$^{2+}$), which were obtained by reacting their neutral bis(carbinol) precursors with Brookhart's acid $H(OEt_2)^+[B\{C_6H_3(CF_3)_2\text{-}3,5\}_4]^-$.[10] The dicationic ferrocene derivatives **1b**$^{2+}$ and **1c**$^{2+}$ seem to be the most electron poor ferrocenes reported to date. Thus, the half-wave potentials of the ferrocene-based oxidation resemble or are even positive of that of the second oxidation of ferrocene itself, i.e. the $Cp_2Fe^{+/2+}$ redox couple under similar conditions.[18] The high Lewis acidity of these compounds becomes manifest through the bleach of the aryl→methylium charge-transfer band in donor solvents, which evidences the formation of Lewis acid/base pairs with the respective solvent as the Lewis base. This leads to pronounced solvatochromism. Reduction of the complexes occurs as two consecutive one-electron steps with a large redox splitting $\Delta E_{1/2}$ of 405 to 740 mV. Nevertheless, no intervalence charge-transfer band for electron transfer from the reduced triarylmethyl to the remaining oxidized triarylmethylium entity was observed, although the ferrocene-1,1′-diyl scaffold might be expected to support through-space electronic coupling by cofacial stacking of these substituents.

Like their monotritylium-substituted counterparts **2a**$^{\bullet}$**–2c**$^{\bullet}$ (Scheme 2), reduced **1a-c**$^{\bullet+/0}$ tend to dimerize/oligomerize via their triarylmethyl centers with concomitant formation of C–C bonds. This tendency is attenuated for the radical cations, which is likely due to electrostatic repulsion between the remaining triarylmethylium centers. Direduced, anisyl-substituted **1b** was found to be reactive towards molecular oxygen and to form a novel peroxo-(bisdiarylmethyl)[4]ferrocenophane with a $–Ar_2C–O–O–CAr_2–$ linkage between the two Cp decks. As it was shown by X-ray crystallography, the four-atom linker induces an only moderate ring strain as revealed by a 7.2° tilt between the Cp rings.

Another intriguing finding of this study is that anisyl-substituted **1b**$^{2+}$ exists as a mixture of a diamagnetic and a paramagnetic form. These two isomers interconvert via a sizeable energy barrier, which gives rise to hysteresis. The paramagnetic form is obviously the result of an electron transfer from the ferrocene nucleus to one of the triarylmethylium centers. Such behavior of **1b**$^{2+}$ is reminiscent of a magnetochemical switch, where, by action of an external trigger, a diamagnetic state can be altered into a diradical state with two unpaired spins. Further work in our laboratories is directed to exploring this prospect further.

Experimental Section

General Methods: All manipulations were carried out at room temperature in a nitrogen atmosphere using standard Schlenk techniques, unless stated otherwise. Solvents were dried and distilled by standard procedures and degassed by saturation with nitrogen prior to use. Ferrocene-1,1′-dicarboxylic acid was prepared according to a literature procedure[31] and converted to its dimethyl ester following the procedure procured for ferrocene carboxylic acid.[32] ^{1}H NMR (400 MHz), $^{13}C\{^1H\}$ NMR (101 MHz) and $^{31}P\{^1H\}$ NMR (162 MHz) spectra of the compounds were measured on a Bruker Avance III 400 spectrometer at room temperature in the indicated deuterated solvent. The spectra were referenced to the signal of residual protonated solvent (^{1}H) or the solvent signal (^{13}C). UV/Vis/NIR spectra were recorded on a TIDAS fiber optic diode array spectrometer (combined MCS UV/NIR and PGS NIR instrumentation) from j&m in HELLMA quartz cuvettes with 0.1 cm optical path lengths.

All electrochemical experiments were executed in a custom-built cylindrical vacuum-tight one-compartment cell. A spiral-shaped Pt wire and a Ag wire as the counter and pseudoreference electrodes were sealed into glass capillaries and fixed by Quickfit screws via standard joints. A platinum electrode was introduced as the working electrode through the top port via a Teflon screw cap with a suitable fitting. It was polished with first 1 μm and then 0.25 μm diamond paste before measurements. The cell was attached to a conventional Schlenk line via a side

arm equipped with a Teflon screw valve, allowing experiments to be performed under an argon atmosphere with approximately 5 mL of analyte solution. NBu_4^+ $[B\{C_6H_3(CF_3)_2\}_4]^-$ (0.02 M) was used as the supporting electrolyte. Referencing was done with addition of an appropriate amount of decamethylferrocene (Cp^*_2Fe, $E_{1/2}$ = –550 mV with respect to Cp_2Fe) as an internal standard to the analyte solution after all data of interest had been acquired. Representative sets of scans were repeated with the added standard. Electrochemical data were acquired with a computer controlled BASi CV50 potentiostat.

The optically transparent thin-layer electrochemical (OTTLE) cell was also custom-built according to the design of *Hartl* et al.[33] It consists of a Pt working and counter electrode and a thin silver wire as a pseudoreference electrode sandwiched between two CaF_2 windows of a conventional liquid IR cell. The working electrode is positioned in the center of the spectrometer beam. Electron paramagnetic resonance (EPR) studies were performed on a MiniScope MS 400 Table-top X-band spectrometer from Magnettech.

X-ray diffraction analysis was performed at 100 K on a STOE IPDS-II diffractometer equipped with a graphite-monochromated radiation source (λ = 0.71073 Å) and an image plate detection system. A yellow, blocky crystal of **1b-O$_2$** obtained from slow evaporation of a solution of this complex in CH_2Cl_2 was mounted on a fine glass fiber with silicon grease. The selection, integration, and averaging procedure of the measured reflection intensities, the determination of the unit cell dimensions and a least-squares fit of the 2θ values as well as data reduction, LP-correction and space group determination were performed using the X-Area software package delivered with the diffractometer. A semiempirical absorption correction was performed.[34] The structure was solved by the heavy-atom method. Structure solution was completed with difference Fourier syntheses and full-matrix least-squares refinements using SHELX-2017[35] and OLEX2,[36] minimizing $\omega(F_o^2 - F_c^2)^2$. The weighted R factor (wR^2) and the goodness of the fit GOOF are based on F^2. All non-hydrogen atoms were refined with anisotropic displacement parameters, while hydrogen atoms were introduced in a riding model.

Crystallographic data (excluding structure factors) for the structure in this paper have been deposited with the Cambridge Crystallographic Data Centre, CCDC, 12 Union Road, Cambridge CB21EZ, UK. Copies of the data can be obtained free of charge on quoting the depository number CCDC-1971352 (Fax: +44-1223-336-033; E-Mail: deposit@ccdc.cam.ac.uk, http://www.ccdc.cam.ac.uk).

The ground state electronic structures of the full complexes were calculated by density functional theory (DFT) methods using the GAUSSIAN 09 program package.[37] Geometry optimizations were performed without any symmetry constraints. Open shell systems were calculated by the unrestricted Kohn–Sham approach (UKS). Geometry optimization followed by vibrational analysis was performed in solvent media. Solvent effects were described by the polarizable continuum model (PCM) with standard parameters for 1,2-dichloroethane.[38] For Fe, the ten-electron quasirelativistic effective core potential (ECP) MDF10 was used,[39] and 6-31G(d) polarized double-ξ basis sets[40] were employed together with the Perdew, Burke, Ernzerhof exchange and correlation functional (PBE0).[41] The GaussSum program package was used to analyze the results,[42] while the visualization of the results was performed with the Avogadro program package.[43] Graphical representations of molecular orbitals were generated with the help of GNU Parallel[44] and plotted using the vmd program package[45] in combination with POV-Ray.[46] Electronic transitions were calculated by the time-dependent DFT (TD-DFT) method.

Synthesis and Characterization of 1a(OH)$_2$:

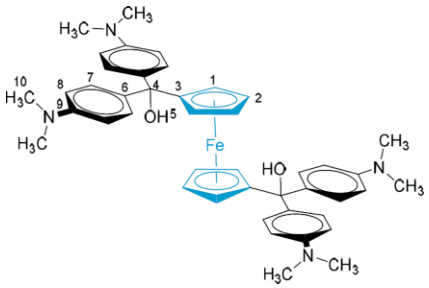

1.39 g (6.95 mmol, 4.2 equiv.) of 4-bromo-*N*,*N*-dimethylaniline were dissolved in 40 mL of dry degassed tetrahydrofuran. 3.9 mL (1.9 M solution in *n*-hexane, 7.3 mmol, 4.4 equiv.) of *t*BuLi were added dropwise to the solution at –78 °C. After stirring for 15 min a solution of 500 mg (1.66 mmol, 1 equiv.) of dimethyl-1,1'-ferrocenedicarboxylate in 30 mL of tetrahydrofuran was added to the reaction mixture at –78 °C. After stirring overnight with slow warming to room temperature, the reaction mixture was quenched with the addition of 40 mL of water and the solvent was removed in vacuo. The residue was dissolved in Et_2O and extracted with water (3 × 50 mL). The aqueous layer was separated off and extracted with Et_2O (3 × 100 mL). The combined organic phases were washed with brine (3 × 20 mL), dried with $MgSO_4$, and the solvent was evaporated in vacuo. The dark green crude product was washed with 210 mL of Et_2O (1 × 150 mL, 3 × 20 mL) to yield 490 mg (0.678 mmol, 41 %) of **1a(OH)$_2$** as a green crystalline solid. **^{1}H NMR** ($CDCl_3$, 400 MHz): δ = 7.12 (d, $^3J_{H,H}$ = 8.8 Hz, 8 H, H7), 6.62 (d, $^3J_{H,H}$ = 8.8 Hz, 8 H, H8), 4.15 (s, 4 H, H1), 3.96 (s, 4 H, H2), 3.84 (s, 2 H, H5), 2.91 (s, 24 H, H10) ppm. **^{13}C NMR** ($CDCl_3$, 101 MHz): δ = 149.4 (C9), 138.8 (C6), 128.1 (C7), 111.7 (C8), 99.0 (C3), 77.7 (C4), 69.5 (C1), 68.1 (C2), 40.8 (C10) ppm.

Synthesis and Characterization of 1a^{2+}·2BAr$_{F24}^-$:

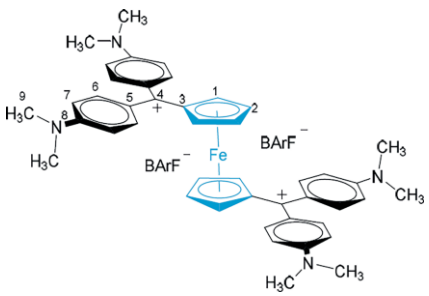

1.100 g (1.01 mmol, 2.05 equiv.) of Brookhart's acid in 40 mL of dry degassed Et_2O were added dropwise to 354 mg (0.49 mmol, 1 equiv.) of **1a(OH)$_2$** in 40 mL of dry degassed Et_2O at room temperature. The reaction mixture turned from green to dark blue. After stirring for 30 min the blue solution was evaporated and the petrol-colored solid was dried in vacuo, yielding 1.18 g (0.489 mmol, quantitative) of **1a^{2+}**. **^{1}H NMR** (CD_2Cl_2, 400 MHz): δ = 7.72 (s, 16 H, BAr_{F24}-CF_3CHCF_3), 7.57 (d, $^3J_{H,H}$ = 9.4 Hz, 8 H, H6), 7.55 (s, 8 H, BAr_{F24}-$CF_3CHCBCHR'$), 6.69 (d, $^3J_{H,H}$ = 9.4 Hz, 8 H, H7), 5.17 (s, 4 H, H1), 4.99 (s, 4 H, H2), 3.15 (s, 24 H, H9). **^{13}C NMR** (CD_2Cl_2, 101 MHz): δ = 181.1 (C4), 161.79 (BAr_{F24}), 156.8 (C8), 139.3 (C6), 134.8 (BAr_{F24}), 127.8 (C5), 117.5 (BAr_{F24}), 112.6 (C7), 84.2 (C3), 79.2 (C2), 77.9 (C1), 40.5 (C9) ppm. **MS** (ESI): calcd. for $C_{44}H_{48}FeN_4$: 344.1607 $[M]^{2+}$; found 344.1478. $C_{108}H_{72}B_2F_{48}FeN_4$: calcd. C, 53.71 %; H, 3.00 %; N, 2.32 % N; found: C, 52.79 %; H, 2.29 %; N, 2.36 %.

Synthesis and Characterization of 1b(OH)$_2$:

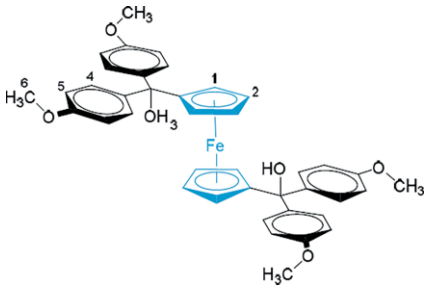

Ferrocene (2.2 g, 12 mmol, 1.5 equiv.) was dissolved in 15 mL of dry THF and cooled to 0 °C. 5.5 mL (1.9 M solution in *n*-hexane, 10.4 mmol, 1.3 equiv.) of *t*BuLi were added dropwise to the solution. After stirring for 15 min, a solution of 1.94 g (8 mmol, 1 equiv.) of 4,4'-dimethoxybenzophenone in 20 mL of tetrahydrofuran was added to the reaction mixture at 0 °C. After stirring for 15 min, the ice bath was removed and the yellow solution was stirred for additional 25 min at room temperature before the reaction mixture was quenched with 30 mL of water and the solvent was removed in vacuo. The residue was dissolved in Et_2O and extracted with water (3 × 50 mL). The aqueous layer was separated off and extracted with Et_2O (3 × 100 mL). The combined organic phases were washed with brine (3 × 20 mL), dried with $MgSO_4$, and the solvent was evaporated in vacuo. The residual solid was purified by column chromatography. A petroleum ether/ethyl acetate (PE/EA) 5/1 mixture eluted some monosubstituted (η^5-C_5H_5)Fe(η^5-$C_5H_4C(C_6H_4OMe\text{-}4)_2OH$ (**2aOH**) and unreacted 4,4'-dimethoxybenzophenone). With pure EA as eluent, the orange band of **1b(OH)$_2$** was eluted. After solvent evaporation, **1b(OH)$_2$** was obtained in the form of dark yellow crystals. The yield was 800 mg (1.2 mmol, 30 % with respect to 4,4'-dimethoxybenzophenone). **^{1}H NMR** ([D$_6$]DMSO, 400 MHz): δ = 7.07 (d, $^3J_{H,H}$ = 8.0 Hz, 8 H, H4), 6.78 (d, $^3J_{H,H}$ = 8.0 Hz, 8 H, H5), 6.02 (s, 2 H, H3), 3.97 (d, $^3J_{H,H}$ = 2.7 Hz, 4 H, H1), 3.91 (d, $^3J_{H,H}$ = 2.7 Hz, 4 H, H1), 3.71 (s, 12 H, H6) ppm. **ESI-MS** (CH_3CN): calcd. for $C_{40}H_{38}FeO_6$: 670.2045 [M] $^+$; found 670.1975.

Synthesis and Characterization of 1b^{2+}·2BAr$_{F24}^-$:

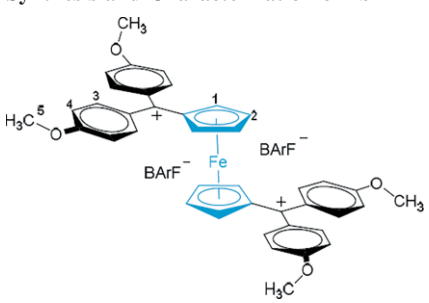

320 mg (0.31 mmol, 2.05 equiv.) of Brookhart's acid in 5 mL of dry degassed Et_2O were added dropwise to 100 mg (0.14 mmol, 1 equiv.) of **1b(OH)$_2$** in 5 mL of dry degassed Et_2O at room temperature. The reaction mixture turned from yellow to dark green. After stirring for 20 min the solvent was removed to obtain **1b^{2+}** as a red solid in quantitative yield. **^{1}H NMR** ($CDCl_3$, 400 MHz): δ = 7.66 (s, 16 H, BArF-$CF_3C\mathit{H}CF_3$), 7.55 (d, $^3J_{H,H}$ = 8.9 Hz, 8 H, H3), 7.47 (s, 8 H, BArF-$CF_3C\mathit{H}CBC\mathit{H}$R'), 6.96 (d, $^3J_{H,H}$ = 8.9 Hz, 8 H, H4), 5.45 (t, $^3J_{H,H}$ = 2.1 Hz, 4 H, H1), 5.10 (t, $^3J_{H,H}$ = 2.1 Hz, 4 H, H2), 3.92 (s, 12 H, H5).

Synthesis and Characterization of 1c(OH)$_2$:

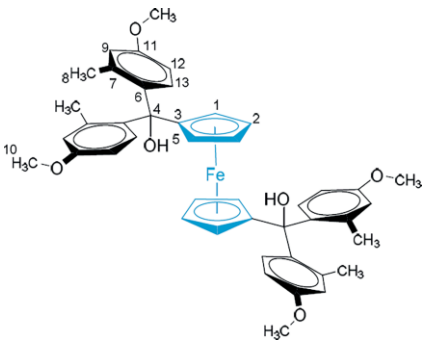

2.10 g (1.5 mL, 10.4 mmol, 4.2 equiv.) of 1-bromo-4-methoxy-1-methyl-benzene were dissolved in 200 mL of dry degassed absolute ether (Et_2O). 3.9 mL of a 1.9 M solution of *t*BuLi in *n*-hexane (7.3 mmol, 4.4 equiv.) were added dropwise to the solution at –78 °C. After stirring for 15 min, a solution of 7.50 g (2.48 mmol, 1 equiv.) of dimethyl-1,1′-ferrocenedicarboxylate in 200 mL of Et_2O was added to the reaction mixture at –78 °C. After stirring overnight, the reaction mixture was quenched with 100 mL of water. The residue was dissolved in Et_2O and extracted with water (3 × 50 mL). The aqueous layer was separated off and extracted with Et_2O (3 × 100 mL). The combined organic phases were washed with brine (3 × 20 mL), dried with $MgSO_4$, and the solvent was evaporated in vacuo. The orange crude product was purified by recrystallization from Et_2O to yield 1.12 g (1.54 mmol, 62 %) of **1c(OH)$_2$** as a yellow crystalline solid. **^{1}H NMR** ($CDCl_3$, 400 MHz): δ = 7.48 (broad s, 4 H, H13), 6.65–6.72 (m, 4 H, H12), 6.55–6.59 (m, 4 H, H9), 4.18 (broad s, 4 H, H1), 4.00 (s, 4 H, H2), 3.99 (s, 2 H, H5), 3.78 (s, 12 H, H10), 1.74 (s, 12 H, H8) ppm. **^{1}H NMR** ([D$_8$]toluene, 400 MHz): δ = 7.65 (broad s, 4 H, H13), 6.58–6.63 (m, 8 H, H9, H12), 4.24 (broad s, 4 H, H1), 3.84 (s, 4 H, H2), 3.75 (s, 2 H, H5), 3.40 (s, 12 H, H10), 1.89 (s, 12 H, H8) ppm. **^{13}C NMR** ($CDCl_3$, 101 MHz): δ = 158.5 (C6), 137.4 (C7), 129.9 (C13), 117.4 (C9), 109.8 (C12), 100.0 (C3), 78.1 (C4), 70.5 (C1), 68.5 (C2), 55.3 (C10), 22.1 (C8).

Synthesis and Characterization of 1c^{2+}·2BAr$_{F24}^-$:

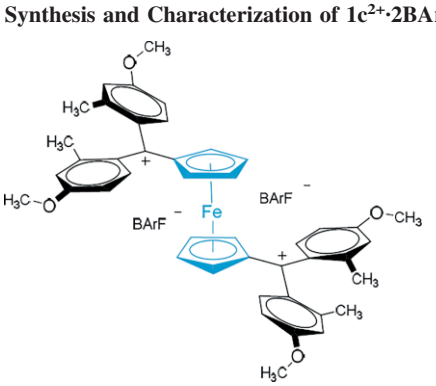

550 mg (0.51 mmol, 2.05 equiv.) of Brookhart's acid in 40 mL of dry degassed Et_2O were added dropwise to 179.4 mg (0.25 mmol, 1 equiv.) of **1c(OH)$_2$** in 40 mL of dry degassed Et_2O at room temperature. The color of the reaction mixture changed from yellow to dark yellow. After stirring for 30 min the solvent was stripped off the ochre solution. The resulting purple solid was dried in vacuo, yielding 590 mg (0.246 mmol, quantitative) of **1c^{2+}**. Due to paramagnetic broadening it was not possible to obtain meaningful NMR spectra. **MS** (ESI): calcd. for $C_{44}H_{44}FeO_4$ 346.1306 $[M]^{2+}$; found 346.1461 (measured in dichlo-

romethane, non-calibrated). $C_{108}H_{68}B_2F_{48}FeO_4$: calcd. 53.62 % C, 2.83 % H; found: 52.71 % C, 3.42 % H.

Synthesis and Characterization of 1b-O_2:

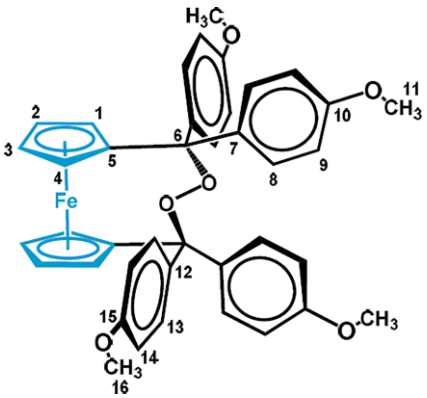

Inside a glove box **1b^{2+}·2BAr$_{F24}^-$** (100 mg, 0.042 mmol, 1 equiv.) was dissolved in 3 mL of degassed CH_2Cl_2 and 16 mg (0.084 mmol, 2 equiv.) of cobaltocene were added. The mixture was stirred for 10 min, then removed from the glove box, exposed to the air and stirred at room temperature overnight. The solvent was evaporated under vacuum and the residue was extracted with *n*-hexane. Evaporation of the solvent gave **1b-O_2** in quantitative yield. **^{1}H NMR** (400 MHz, C6D6): δ = 7.87 (d, 4 H, ^{3}*JHH* = 8.85 Hz, H8), 7.35 (d, 4 H, $^3J_{HH}$ = 8.85 Hz, H13), 6.90 (d, 4 H, $^3J_{HH}$ = 8.85 Hz, H9), 6.52 (d, 4 H, $^3J_{HH}$ = 8.85 Hz, H14), 5.11 (m, 2 H, H1), 4.21 (m, 2 H, H2), 4.03 (m, 2 H, H4), 3.91 (m, 2 H, H3), 3.33 (s, 6 H, CH3–11), 3.21 (s, 6 H, CH3–16). **^{13}C NMR** (C6D6, 101 MHz): δ = 159.3 (C10), 158.9 (C15), 136.9 (C12), 136.4 (C7), 130.3 (C8), 128.1 (C13), 113.5 (C14), 113.4 (C9), 94.2 (C5), 89.9 (C6), 75.1 (C4), 71.7 (C1), 70.2 (C2), 67.6 (C3), 54.8 (C11), 54.7 (C16). **ESI-MS** (CH_3CN) calcd. for $C_{40}H_{36}FeO_6$+H$^+$ [MH]$^+$ 669.1915; found 669.1925.

Synthesis and Characterization of 1b-HOH:

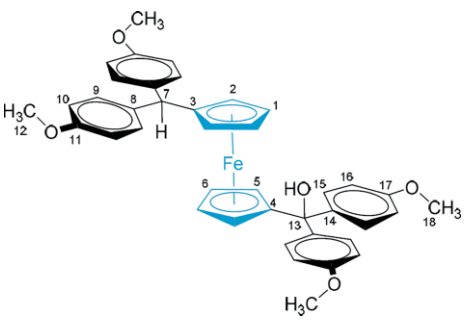

Inside a glove box **1b^{2+}·2BAr$_{F24}^-$** (100 mg, 0.042 mmol, 1 equiv.) was dissolved in 3 mL of degassed CH_2Cl_2. 16 mg (0.084 mmol, 2 equiv.) of cobaltocene and 0.76 µL of water were added and the mixture was allowed to stir at room temperature for 2 h. During this time the solution turned green. The solvents were removed under reduced pressure and the green solid was extracted with *n*-hexane. Solvent was stripped off the filtered extract and the solid residue was purified by solvent chromatography (silica, PE/EA 5/1). The first fraction contained small quantities of 6,6-diansiylfluorene. The second, orange band provided complex **1b-HOH** after solvent evaporation and washing with cold *n*-pentane. **^{1}H NMR** (400 MHz, C_6D_6): δ = 7.41 (d, 4 H, $^3J_{HH}$ = 8.80 Hz, H15), 7.04 (d, 4 H, $^3J_{HH}$ = 8.85 Hz, H9), 6.76 (d, 4 H, $^3J_{HH}$ = 8.80 Hz, H16), 6.74 (d, 4 H, $^3J_{HH}$ = 8.85 Hz, H10), 4.81 (s, 1 H, H7), 4.07 (m, 2 H, H2), 4.03 (m, 2 H, H1), 4.02 (m, 2 H, H5), 3.92 (m, 2 H, H6), 3.32 (s, 12 H, H12, H18), 3.01 (s, 1 H, OH). ^{13}C NMR (100.61 MHz, C_6D_6): δ = 158.6 (C17), 158.2 (C11), 140.4 (C14), 137.6 (C8), 129.6 (C9), 128.5 (C15), 113.5 (C10), 112.8 (C16), 100.2 (C4), 93.2 (C3), 76.9 (C13), 69.5 (C2), 69.4 (C5), 68.9 (C6), 68.2 (C1), 54.4 (C12, C18), 49.9 (C7). **ESI-MS** (CH_3CN) calcd. for $C_{40}H_{38}FeO_5$: [M]$^+$ 654.2071; found: 654.1662; [M-OH]$^+$ 637.2077; found: 637.1668.

Supporting Information (see footnote on the first page of this article): NMR spectra of the complexes, UV/Vis/NIR spectra of the reduced forms of complexes **1b^{2+}** and **1c^{2+}**, ESI-MS of complexes **1b-O_2** and **1b-HOH**, Tables with UV/Vis data in various solvents and details of the crystallographic structure determination as well as the bond lengths and bond angles.

Acknowledgements

We gratefully acknowledge financial support of this work by the Deutsche Forschungsgemeinschaft (DFG) (grant no. Wi1262/9–2). *Larissa A. Casper* thanks the Studienstiftung des Deutschen Volkes for a PhD grant. We are also grateful to the DFG and the State of Baden-Württemberg for providing us with access to the computational facilities of the JUSTUS HPC facilities as a part of the bw_FOR network at the University of Ulm (grant no. INST 40/467–1 FUGG). We also thank *Eva Schiebel* for the synthesis of compound **1b-(OH)$_2$** as a part of an internship. Open access funding enabled and organized by Projekt DEAL.

Keywords: Ferrocene; Tritylium; Electrochemistry; Spectroelectrochemistry; Ferrocenophane; Peroxo compound; EPR spectroscopy; Solvatochromism

References

[1] a) J. H. Richards, E. A. Hill, *J. Am. Chem. Soc.* **1959**, *81*, 3484–3485; b) E. A. Hill, R. Wiesner, *J. Am. Chem. Soc.* **1969**, *91*, 509–510; c) E. A. Hill, J. H. Richards, *J. Am. Chem. Soc.* **1961**, *83*, 4216–4221; d) E. A. Hill, J. H. Richards, *J. Am. Chem. Soc.* **1961**, *83*, 3840–3846; e) M. Cais, *Organomet. Chem. Rev.* **1966**, *1*, 435–454; f) W. E. Watts, *J. Organomet. Chem.* **1981**, *220*, 165–172.
[2] U. Behrens, *J. Organomet. Chem.* **1979**, *182*, 89–98.
[3] R. Gleiter, R. Seeger, *Helv. Chim. Acta* **1971**, *54*, 1217–1220.
[4] T. D. Turbitt, W. E. Watts, *J. Chem. Soc. Perkin Trans. 2* **1974**, 177–184.
[5] a) T. D. Turbitt, W. E. Watts, *J. Chem. Soc. Perkin Trans. 2* **1974**, 185–189; b) D. Hellwinkel, H. Fritsch, *Chem. Ber.* **1989**, *122*, 2351–2359; c) C. Arbez-Gindre, B. R. Steele, G. A. Heropoulos, C. G. Screttas, J.-E. Communal, W. J. Blau, I. Ledoux-Rak, *J. Organomet. Chem.* **2005**, *690*, 1620–1626; d) C. Villalonga-Barber, B. R. Steele, V. Kovač, M. Micha-Screttas, C. G. Screttas, *J. Organomet. Chem.* **2006**, *691*, 2785–2792; e) C. Villalonga-Barber, K. Vallianatou, S. Georgakopoulos, B. R. Steele, M. Micha-Screttas, E. Levin, N. Gabriel Lemcoff, *Tetrahedron* **2013**, *69*, 3885–3895.
[6] S. Oßwald, L. A. Casper, P. Anders, E. Schiebel, S. Demeshko, R. F. Winter, *Chem. Eur. J.* **2018**, *24*, 12524–12538.
[7] C. U. Pittman, *Tetrahedron Lett.* **1967**, *8*, 3619–3623.
[8] C. R. Jablonski, *J. Organomet. Chem.* **1979**, *174*, C3-C10.
[9] K. Gonsalves, L. Zhan-Ru, M. D. Rausch, *J. Am. Chem. Soc.* **1984**, *106*, 3862–3863.
[10] M. Brookhart, B. Grant, A. F. Volpe, *Organometallics* **1992**, *11*, 3920–3922.
[11] H. Nishida, N. Takada, M. Yoshimura, T. Sonoda, H. Kobayashi, *Bull. Chem. Soc. Jpn.* **1984**, *57*, 2600–2604.

[12] a) R. J. LeSuer, C. Buttolph, W. E. Geiger, *Anal. Chem.* **2004**, *76*, 6395–6401; b) F. Barrière, W. E. Geiger, *J. Am. Chem. Soc.* **2006**, *128*, 3980–3989; c) A. Hildebrandt, H. Lang, *Organometallics* **2013**, *32*, 5640–5653.
[13] a) I. Ratera, D. Ruiz-Molina, F. Renz, J. Ensling, K. Wurst, C. Rovira, P. Guetlich, J. Veciana, *J. Am. Chem. Soc.* **2003**, *125*, 1462–1463; b) I. Ratera, C. Sporer, D. Ruiz-Molina, N. Ventosa, J. Baggerman, A. M. Brouwer, C. Rovira, J. Veciana, *J. Am. Chem. Soc.* **2007**, *129*, 6117–6129; c) G. D'Avino, L. Grisanti, J. Guasch, I. Ratera, J. Veciana, A. Painelli, *J. Am. Chem. Soc.* **2008**, *130*, 12064–12072; d) J. Guasch, L. Grisanti, S. Jung, D. Morales, G. D'Avino, M. Souto, X. Fontrodona, A. Painelli, F. Renz, I. Ratera, J. Veciana, *Chem. Mater.* **2013**, *25*, 808–814; e) M. Souto, D. C. Morales, J. Guasch, I. Ratera, C. Rovira, A. Painelli, J. Veciana, *J. Phys. Org. Chem.* **2014**, *27*, 465–469.
[14] a) A. S. Ferguson, G. Hallas, *J. Soc. Dyers Colour.* **1973**, *89*, 22–24; b) G. Hallas, K. N. Paskins, D. R. Waring, J. R. Humpston, A. M. Jones, *J. Chem. Soc. Perkin Trans. 2* **1977**, 450–456; c) D. F. Duxbury, *Chem. Rev.* **1993**, *93*, 381–433.
[15] V. Gutmann, *Coord. Chem. Rev.* **1976**, *18*, 225–255.
[16] S. D. Waniek, J. Klett, C. Foerster, K. Heinze, *Beilstein J. Org. Chem.* **2018**, *14*, 1004–1015.
[17] A. Hildebrandt, K. Al Khalyfeh, D. Schaarschmidt, M. Korb, *J. Organomet. Chem.* **2016**, *804*, 87–94.
[18] P. R. Sharp, A. J. Bard, *Inorg. Chem.* **1983**, *22*, 2689–2693.
[19] a) J.-M. Lü, S. V. Rosokha, J. K. Kochi, *J. Am. Chem. Soc.* **2003**, *125*, 12161–12171; b) J.-M. Lü, S. V. Rosokha, I. S. Neretin, J. K. Kochi, *J. Am. Chem. Soc.* **2006**, *128*, 16708–16719; c) S. V. Rosokha, J. K. Kochi, *J. Am. Chem. Soc.* **2007**, *129*, 3683–3697; d) S. V. Rosokha, I. S. Neretin, D. Sun, J. K. Kochi, *J. Am. Chem. Soc.* **2006**, *128*, 9394–9407; e) A. C. Benniston, G. Copley, A. Harriman, D. Howgego, R. W. Harrington, W. Clegg, *J. Org. Chem.* **2010**, *75*, 2018–2027; f) T. Nishinaga, Y. Kanzaki, D. Shiomi, K. Matsuda, S. Suzuki, K. Okada, *Chem. Eur. J.* **2018**, *24*, 11717–11728.
[20] a) W. J. van der Hart, *Mol. Phys.* **1970**, *19*, 75–84; b) K. Ishizu, K. Mukai, A. Shibayama, K. Kondo, *Bull. Chem. Soc. Jpn.* **1977**, *50*, 2269–2271; c) N. I. Tzerpos, A. K. Zarkadis, R. P. Kreher, L. Repas, M. Lehnig, *J. Chem. Soc. Perkin Trans. 2* **1995**, 755–761.
[21] S. P. Solodovnikov, A. Z. Kreindlin, L. S. Shilovtseva, M. I. Rybinskaya, *Organomet. Chem. USSR* **1991**, *4*, 142–145.
[22] J. Jeffery, R. J. Mawby, M. B. Hursthouse, N. P. C. Walker, *J. Chem. Soc., Chem. Commun.* **1982**, 1411–1412.
[23] J. Jeffery, E. J. Probitts, R. J. Mawby, *J. Chem. Soc., Dalton Trans.* **1984**, 2423–2427.
[24] M. Hisatome, S. Minagawa, K. Yamakawa, *J. Organomet. Chem.* **1973**, *55*, c82-c84.
[25] M. Gomberg, *J. Am. Chem. Soc.* **1903**, *25*, 1274–1277.
[26] a) M. Görmen, P. Pigeon, E. A. Hillard, A. Vessières, M. Huché, M.-A. Richard, M. J. McGlinchey, S. Top, G. Jaouen, *Organometallics* **2012**, *31*, 5856–5866; b) M. Hisatome, K. Nakanishi, K. Yamakawa, K. Kozawa, T. Ucnida, *Bull. Chem. Soc. Jpn.* **1992**, *65*, 3275–3281; c) K.-L. Gibis, G. Helmchen, G. Huttner, L. Zsolnai, *J. Organomet. Chem.* **1993**, *445*, 181–186; d) R. M. Gleixner, K. M. Joly, M. Tremayne, B. M. Kariuki, L. Male, D. M. Coe, L. R. Cox, *Chem. Eur. J.* **2010**, *16*, 5769–5777.
[27] M. Roemer, D. Heinrich, Y. K. Kang, Y. K. Chung, D. Lentz, *Organometallics* **2012**, *31*, 1500–1510.
[28] S. Harthong, R. Bach, C. Besnard, L. Guénée, J. Lacour, *Synthesis* **2013**, *45*, 2070–2078.
[29] F. Edelmann, B. Lubke, U. Behrens, *Chem. Ber.* **1982**, *115*, 1325–1331.
[30] a) S. Fox, J. P. Dunne, M. Tacke, D. Schmitz, R. Dronskowski, *Eur. J. Inorg. Chem.* **2002**, *2002*, 3039–3046; b) R. Teuber, R. Köppe, G. Linti, M. Tacke, *J. Organomet. Chem.* **1997**, *545–546*, 105–110.
[31] H. S. Sørensen, J. Larsen, B. S. Rasmussen, B. Laursen, S. G. Hansen, T. Skrydstrup, C. Amatore, A. Jutand, *Organometallics* **2002**, *21*, 5243–5253.
[32] P. Witte, T. K. Lal, R. M. Waymouth, *Organometallics* **1999**, *18*, 4147–4155.
[33] M. Krejcik, M. Danek, F. Hartl, *J. Electroanal. Chem.* **1991**, *317*, 179–187.
[34] W. Herrendorf, W. Bärnighausen, Version 1.06 ed., Fa. Stoe, Darmstadt, Karlsruhe, Gießen, **1999**.
[35] G. M. Sheldrick, *Acta Crystallogr., Sect. A* **2015**, *71*, 3–8.
[36] O. V. Dolomanov, L. J. Bourhis, R. J. Gildea, J. A. K. Howard, H. Puschmann, *J. Appl. Crystallogr.* **2009**, *42*, 339–341.
[37] M. J. Frisch, G. Trucks, H. B. Schlegel, G. E. Scuseria, M. A. Robb, J. R. Cheeseman, G. Scalmani, V. Barone, G. A. Petersson, H. Nakatsuji, M. Caricato, A. Marenich, J. Blonio, B. G. Janesko, R. Gomperts, B. Mennucci, H. P. Hratchian, J. V. Ortiz, A. F. Izmaylov, J. L. Sonnenberg, D. Williams-Young, F. Ding, F. Lipparini, F. Egidi, J. Goings, B. Peng, A. Petrone, T. Henderson, D. Ranasinghe, V. G. Zakrzewski, J. Gao, N. Rega, G. Zheng, W. Liang, M. Hada, M. Ehara, K. Toyota, R. Fukuda, J. Hasegawa, M. Ishida, T. Nakajima, Y. Honda, O. Kitao, H. Nakai, T. Vreven, K. Throssell, J. J. A. Montgomery, J. E. Peralta, F. Ogliaro, M. Bearpark, J. J. Heyd, E. Brothers, K. N. Kudin, V. N. Staroverov, T. Keith, R. Kobayashi, J. Normand, K. Raghavachari, A. Rendell, J. C. Burant, S. S. Iyengar, J. Tomasi, M. Cossi, J. M. Millam, M. Klene, C. Adamo, R. Cammi, J. W. Ochterski, R. L. Martin, K. Morokuma, O. Farkas, J. B. Foresman, D. J. Fox, *Vol. 2016*, Gaussian, Inc., Wallingford CT, **2016**.
[38] M. Cossi, N. Rega, G. Scalmani, V. Barone, *J. Comput. Chem.* **2003**, *24*, 669–681.
[39] M. Dolg, U. Wedig, H. Stoll, H. Preuss, *J. Chem. Phys.* **1987**, *86*, 866–872.
[40] P. H. Hariharan, J. A. Pople, *Theor. Chim. Acta* **1973**, *28*, 213–222.
[41] a) J. P. Perdew, K. Burke, M. Enzerhof, *Phys. Rev. Lett.* **1996**, *77*, 3865–3868; b) C. Adamo, V. Barone, *J. Chem. Phys.* **1999**, *110*, 6158–6170.
[42] N. M. O'Boyle, A. L. Tenderholt, K. M. Langner, *J. Comput. Chem.* **2008**, *29*, 839–845.
[43] a) M. D. Hanwell, D. E. Curtis, D. C. Lonie, T. Vandermeersch, E. Zurek, G. R. Hutchinson, *J. Cheminf.* **2012**, *4*, 17; b) in http://avogadro.cc/.
[44] O. Tange, *USENIX Magazine* **2011**, *36*, 42–47.
[45] W. Humphrey, A. Dalke, K. Schulten, *J. Mol. Graph.* **1996**, *14*, 33–38.
[46] http://www.povray.org/download/, **2004**.

Received: December 19, 2019
Published Online: March 3, 2020

